

Improved Hole Extraction Selectivity of Polymer Solar Cells by Combining PEDOT:PSS with WO₃

Aurelien Sokeng Djoumessi,* Shahidul Alam, Jose Prince Madalaimuthu, Aman Anand, Josef Slowik, Theo Pflug, Rico Meitzner, Roland Roesch, Enrico Gnecco, Alexander Horn, Ulrich S. Schubert, and Harald Hoppe*

As the device performance and stability of polymer solar cells strongly depend on the interfacial charge extraction layers, the hole transport layer (HTL) properties are crucial. Furthermore, unfavorable interactions with the electrode or the photoactive layer should be screened and prevented. Organic solar cells of conventional architecture by varying the HTL material and layer stack systematically between PEDOT:PSS and a sol-gel-derived tungsten oxide (WO₃) are investigated. The impact of various HTLs in the solar cells is investigated by optical and electrical characterization. Interestingly, a triple-layer WO₃/PEDOT:PSS/WO₃ configuration results in the best device performance specifically compared with the use of pristine WO₃ and pristine PEDOT:PSS hole extraction layers. The triple layer also shows an increased reproducibility in the lifetime, which, combined with the improvement in the efficiency, can be the keys for expectable revenue.

mainly due to the development of new photoactive materials and increasing understanding of and control over the morphology of the solar cell's active layer.^[2–4] However, further research is still required to address the three main objectives of OPV advancement: high efficiency, long lifetime, and low cost. An important role in device performance and stability is played by interfacial layers. Generally, poly(3,4-ethylenedioxy thiophene):polystyrene sulfonate (PEDOT:PSS) is the most commonly used hole transport layer (HTL) for extracting the holes from the photoactive layer (PAL) into the conductive transparent electrode. On the one hand, PEDOT:PSS has the advantage of being solution processable at room temperature, but on the other hand, this material is also known to contribute to device degradation by unwanted reactions with the photoactive material and indium tin oxide (ITO) anode in the conventional architecture.^[5–10] Alternatively to PEDOT:PSS, several solution-processable metal oxides (NiO_x, MoO_x, and WO₃) have been introduced, either directly as crystalline nanoparticles or derived from sol-gel processes.^[11–14] They combine the advantages of simple synthesis, high optical transparency, and good environmental stability. Although it is still not easy


material is also known to contribute to device degradation by unwanted reactions with the photoactive material and indium tin oxide (ITO) anode in the conventional architecture.^[5–10] Alternatively to PEDOT:PSS, several solution-processable metal oxides (NiO_x, MoO_x, and WO₃) have been introduced, either directly as crystalline nanoparticles or derived from sol-gel processes.^[11–14] They combine the advantages of simple synthesis, high optical transparency, and good environmental stability. Although it is still not easy

1. Introduction

Organic photovoltaics (OPV) represents a promising technology with high potential in the solar energy sector, and it has attracted a lot of scientific and industrial interest. Currently, the record power conversion efficiency (PCE) for single-junction organic solar cells has reached 18.2%.^[1] This progress is the result of great effort,

A. Sokeng Djoumessi, S. Alam, J. P. Madalaimuthu, A. Anand, J. Slowik, R. Meitzner, R. Roesch, U. S. Schubert, H. Hoppe
Center for Energy and Environmental Chemistry Jena (CEEC Jena)
Friedrich Schiller University Jena
Philosophenweg 7a, 07743 Jena, Germany
E-mail: aurelien.sokengdjoumessi@uni-jena.de;
harald.hoppe@uni-jena.de

A. Sokeng Djoumessi, S. Alam, J. P. Madalaimuthu, A. Anand, J. Slowik, R. Meitzner, R. Roesch, U. S. Schubert, H. Hoppe
Laboratory of Organic and Macromolecular Chemistry (IOMC)
Friedrich Schiller University Jena
Humboldtstrasse 10, 07743 Jena, Germany

 The ORCID identification number(s) for the author(s) of this article can be found under <https://doi.org/10.1002/ente.202100474>.

© 2021 The Authors. Energy Technology published by Wiley-VCH GmbH. This is an open access article under the terms of the Creative Commons Attribution-NonCommercial-NoDerivs License, which permits use and distribution in any medium, provided the original work is properly cited, the use is non-commercial and no modifications or adaptations are made.

DOI: 10.1002/ente.202100474

J. P. Madalaimuthu
Abbe School of Photonics
Friedrich Schiller University Jena
Albert-Einstein-Straße 6, 07743 Jena, Germany

T. Pflug, A. Horn
Lasereinstitut Hochschule Mittweida
Hochschule Mittweida
Schillerstraße 10, 09648 Mittweida, Germany

T. Pflug
Institut für Physik
Technische Universität Chemnitz
Reichenhainer Straße 70, 09126 Chemnitz, Germany

E. Gnecco
Otto Schott Institute of Materials Research
Friedrich Schiller University Jena
Löbdergraben 32, 07743 Jena, Germany

to control their work function, their use contributes to achieving good ohmic contact and improving the long-term stability of polymer solar cells (PSCs).^[15,16] Previous works on WO₃ as the hole injection layer in the light-emitting diode^[17] and as HTL in PSCs are already reported and the deposition was either by vacuum or by solution processing. Thermally evaporated and deposited WO₃ was investigated as a replacement of PEDOT:PSS in poly(3-hexylthiophene-2,5-diyl):phenyl-C₆₀-butyric acid methyl ester (P3HT:PC₆₁BM)-based solar cells and an enhancement of the photovoltaic performance was reported.^[18,19] Varnamkhasti et al. also showed that thermally evaporated WO₃ and copper phthalocyanine (CuPc) that were deposited in a bilayer HTL configuration contributed to improving the performance of the device by increasing the charge injection and reducing the series resistance.^[20] However, the high vacuum deposition of WO₃ is more expensive and energy intensive than solution-processed WO₃, which reveals the advantage of being compatible with the roll-to-roll fabrication technology of PSCs under atmospheric conditions. Many research groups reported the use in the inverted configuration of solution-processed WO₃ prepared by sol-gel technique, nanoparticle dispersion, and blending with PEDOT:PSS solution.^[13,21–23] For conventional architecture devices, Tan et al. reported a higher performance for the solar cell prepared from tungsten (VI) isopropoxide solution in isopropanol as a precursor coated and annealed on ITO glass compared with a PEDOT:PSS device.^[24] The same sol-gel technique was used by Qiu et al. and the authors reported both performance and lifetime improvement in the device with WO₃ precursor solution layer treated by O₂ plasma.^[25] Choi et al. proceeded with a new approach of sol-gel preparation of WO₃ solution by diluting tungsten (VI) ethoxide solution in ethanol. The device fabricated by this sol-gel precursor solution was reported to feature a comparable performance and better stability

than the PEDOT:PSS device.^[14] Finally, Kim et al. prepared another sol-gel solution type by dissolving tungsten powder in hydrogen peroxide (H₂O₂) solution. The prepared WO₃ solution diluted with isopropanol was intercalated between the ITO anode and the PEDOT:PSS in a way to prevent possible reactions between them, and the fabricated solar cell device was reported to be better performing and more stable than the device with PEDOT:PSS only.^[26]

In this contribution, a new sol-gel technique for WO₃ coatings is introduced, and poly[*N*-9'-heptadecanyl-2,7-carbazole-alt-5,5-(4',7'-di-2-thienyl-2',1',3'-benzothiadiazole)]: phenyl-C₇₀-butyric acid methyl ester (PCDTBT:PC₇₁BM) solar cells are fabricated using PEDOT:PSS and tungsten oxide (WO₃) as HTL materials in various configurations. Both constituents were deposited on top of the glass/ITO substrates either individually, or by blending, or in layer-by-layer stacks. Kelvin probe (KP) measurements were applied to investigate the work function of hole extraction layers, showing unexpected results for the layer stacks. Thorough characterization of the completed solar cells provided further insight into the working mechanism of the hole extraction layers.

2. Experimental Section

2.1. Materials

All materials were used as received, and the chemical structures of the donor and acceptor materials are shown in **Figure 1a**. The donor material poly[*N*-9'-heptadecanyl-2,7-carbazole-alt-5,5-(4',7'-di-2-thienyl-2',1',3'-benzothiadiazole)] (PCDTBT) was purchased from 1-Material and the fullerene acceptor phenyl-C₇₀-butyric acid methyl ester (PC₇₁BM) was purchased from Solenne BV.

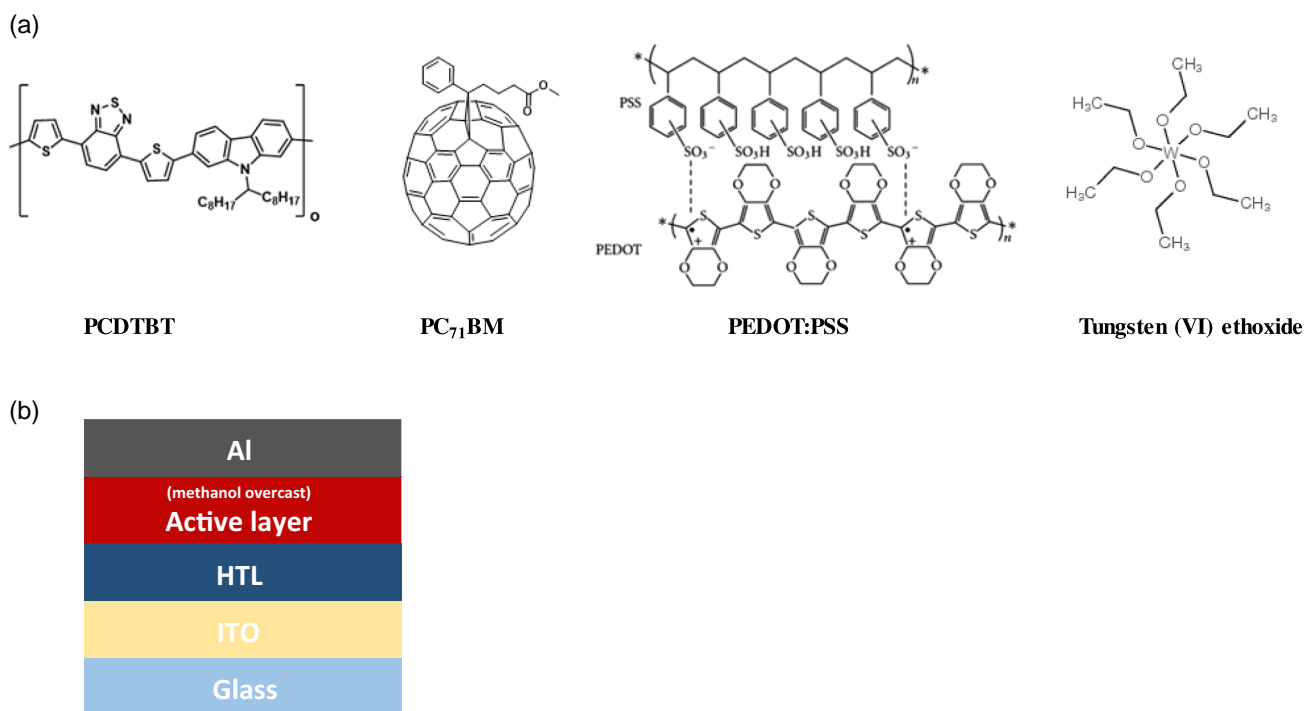


Figure 1. a) Schematic representation of the chemical structures of the materials used and b) representation of the solar cell layer stack.

PCDTBT:PC₇₁BM solution was prepared by dissolving one part of PCDTBT with two parts of PC₇₁BM (1:2 weight ratio) in a chlorobenzene:chloroform (1:1) mixture. The 1.5 wt% blend active material solution was stored inside the glovebox at 50 °C on a hotplate and continuously stirred at 750 rpm for 2 weeks.

Poly(3,4-ethylenedioxythiophene):polystyrene sulfonate (PEDOT:PSS) (Clevios P VP Al4083) was purchased from Heraeus and used as a hole transporting/extraction layer (HTL). A tungsten oxide precursor solution was prepared from tungsten (VI) ethoxide (purchased from Alfa Aesar) and methoxy ethanol. Tungsten (VI) ethoxide (270 mg) were dissolved in methoxy ethanol (75 mL) by vigorous stirring and was filled into a three-necked round-bottomed flask, both under inert atmosphere. Next, the flask was attached to a water-cooled reflux condenser and dipped into a heated oil bath. Before closing all the openings of the flask and the condenser tightly, a thermometer and a magnetic stir bar were submerged in the solution and the air was dispelled from the whole system by pure nitrogen gas flow. Then, the solution was stirred at 80 °C for 1 h, followed by 120 °C for 2 h, followed by 80 °C for 2 h, and finally 120 °C for 1 h. Between each of these steps, heating or cooling phases of 30 min each were necessary. After the final rapid cooling of the solution to room temperature, the flask was opened, and the final precursor solution was transferred into a clean bottle. The precursor solution was thereafter stored under inert atmosphere. The precursor solution for tungsten oxide (WO₃) was then diluted in isopropanol to 15% v/v and used as an HTL as well as a blend component (this diluted WO₃ solution) within the PEDOT:PSS solution in a 50% v/v (1:1 ratio).

2.2. Device Preparation

The fabrication of solar cells started with cleaning of indium tin oxide (ITO)-coated glasses (with a sheet resistance of 10 Ω sq⁻¹) in an ultrasonic bath successively using toluene and isopropanol for 15 min each. All the devices were prepared in a conventional architecture. The substrates were first dried with a nitrogen-air blowing gun before the spin coating of the HTL. As HTLs, pristine PEDOT:PSS, pristine WO₃, and the blend PEDOT:PSS:WO₃ were used. Both pristine materials were also deposited layer by layer. An overview of the different HTLs used in this study is shown in **Table 1**. PEDOT:PSS and the blended PEDOT:PSS:WO₃ were spin coated at 3000 rpm, and afterward the samples were annealed on a hotplate for 15 min at 178 °C under ambient conditions, to remove residual moisture. The WO₃ precursor solution was spin coated at 1000 rpm, and the samples were annealed at 90 °C for 15 min in the air to activate WO₃, as shown in **Figure 2**. The annealing temperature of the WO₃ precursor solution was chosen based on a

Table 1. Overview of the experimental variation of HTL.

Name	HTL layer stack
HTL 1	PEDOT:PSS
HTL 2	WO ₃
HTL 3	PEDOT:PSS:WO ₃
HTL 4	PEDOT:PSS/WO ₃
HTL 5	WO ₃ /PEDOT:PSS
HTL 6	WO ₃ /PEDOT:PSS/WO ₃

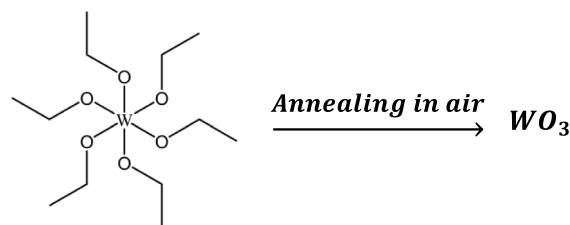


Figure 2. Schematic representation of the activation of WO₃ after annealing of the tungsten (VI) ethoxide.

systematic study of the dependence of annealing temperature, ranging between 90 and 230 °C in 20 °C steps, on the work function of the final WO₃ layer (see Figure S1, Supporting Information). The samples were then immediately transferred to a nitrogen-filled glovebox and cooled down to room temperature before the active layer deposition took place. The active layer solution was deposited at 1200 rpm, and the samples were annealed for 10 min at 80 °C on the hotplate inside the glovebox. After annealing, a methanol solvent overcast was done at 4000 rpm on top of the active layer. Solar cells were completed by depositing 100 nm of aluminum (Al) by physical vapor deposition at less than 10⁻⁶ mbar through a shadow mask to form the back electrode, yielding solar cells with an active area of 0.42 cm². Samples were finally encapsulated under glass to protect the solar cells from water and oxygen using UV-curing glue. The complete device layer stack is shown in Figure 1b.

2.3. Characterization

For standard characterization, the current–voltage (*I*–*V*) measurements of the solar cell devices were carried out under a class A AM1.5 solar simulator (intensity: 100 mW cm⁻²) and in the dark. All the measurements were recorded with a computer-controlled Keithley 2400 source meter unit (SMU).

External quantum efficiency (EQE) was recorded under monochromatic light with an additional halogen bias light, providing an excitation intensity of about 1 sun. A Si detector was used to calibrate the EQE system (Bentham PVE 300).

Electroluminescence spectroscopy (ELS) was conducted on solar cell devices by applying a constant current of 50 mA from a Keithley 2400 SMU, yielding a current density of about 120 mA cm⁻². The emitted light was transmitted via fiber optics to Si (Avantes AvaSpec ULS-2048) and cooled InGaAs (Avantes AvaSpec NIR256-1) fiber spectrometers and measured with an integration time of 10 s.

Light intensity-dependent current-voltage (LID-IV) measurements were carried out by measuring the *I*–*V* characteristics of solar cells upon changing the light intensity from a high-power LED (wavelength: 520 nm) using different neutral optical filters.

For optical characterization, the film photoluminescence spectroscopy (PLS) spectra were recorded with an AvantesAvaSpec ULS-3648 fiber spectrometer with an integration time of 10 s. PL excitation was conducted by a laser diode emitting at 405 nm. Transmittance and reflectance spectra were recorded on the films coated on glass with two Avantes AvaSpec-ULS3648-USB2-UA-25 fiber spectrometers with an integration time of 13 milliseconds, and absorbance was calculated from those values.

Atomic force microscopy (AFM) measurements were carried out in tapping mode with a Nanowizard 4 (JPK Instruments) setup and PPP-NCH-AuD (Nanosensors) probes.

The film thickness was determined on HTLs coated on bare glass. A small area of the thin film was removed by a needle without damaging the substrate. The resulting topology on the edge was measured by laser scanning microscopy (LEXT 3D measuring laser microscope OLS4100, Olympus).

The work function of the varied HTLs was also measured on ITO glass by a single-point KP system from Anfatec. The system was calibrated with freshly cleaved highly oriented pyrolytic graphite (HOPG), whose work function was assumed to be 4.46 eV.

2.4. Aging

Solar cells were aged in a self-built setup with Keithley 2700 including a multiplexer card and Keithley 2400 for I - V sweeps. Sweeps were conducted from -1 to 1 V for I - V characterization. The setup was held at 45°C ambient temperature and illumination was conducted by a white-light LED array, which is compatible with ISOS-L1 conditions.^[27,28] The light intensity was set to a value to achieve a comparable short-circuit current density as under a calibrated solar simulator set to an AM1.5G spectrum with a flux density of 100 mW cm^{-2} .

For the evaluation of the lifetimes, aging curves were fit with a biexponential decay function, and lifetimes and lifetime energy yields (LEY) were evaluated according to Roesch et al.^[29]

3. Results and Discussion

The detailed energy-level diagram of the material used in this work is shown in **Figure 3a**. The results of KP measurements conducted on various HTL stacks are shown in **Figure 3b**. The pristine PEDOT:PSS displayed a WF value of 5.03 eV, which is in the lower end of the expected range for PVP Al4083. The pristine WO_3 and the PEDOT:PSS/ WO_3 blend exhibited even lower values. Upon stacking both materials, the WF was increased, and the triple-layer configuration WO_3 /PEDOT:PSS/ WO_3 featured the highest WF with a value of 5.12 eV.

To have a better understanding of the effect of the HTL variation on the optical properties of the active material PCDTBT:PC₇₁BM, the transmission was evaluated on thin films coated on glass substrates both without and with the PAL on top. **Figure 4a** shows the measured transmittance of all the films and in **Figure 4b** the calculated absorbance ($A = 100 - T - R$) is depicted. There is a slight difference in the absorbance. This result shows that the variation of the different HTLs does not severely affect the morphology of the photoactive material.

Figure 5 shows the corrected PL spectra (corrected by the absorbance at the excitation wavelength of 405 nm of the laser). The PL spectra are also quantitatively in quite good agreement for the different HTL stacks, so that no significant change of the local phase separation in the active layer can be expected.

Regarding electrical characterization, the current-voltage (I - V) characteristics of all the solar cells were measured in the dark and under illumination and the results are shown in **Figure 6**. For the dark J - V characteristics of the reference device with PEDOT:PSS in **Figure 6a**, we have 2.5 orders of magnitude rectification for the reverse and forward currents bias, which corresponds to a good diode behavior. The pristine WO_3 reveals a worse rectification than the PEDOT:PSS device, yielding a higher leakage current or lower shunt resistance. So, the layer shows lower charge carrier selectivity. The blend device yields very similar properties as the pristine PEDOT:PSS device concerning the shunt resistance. For the double-layer devices, there is an improved blocking behavior as well as for the triple-layer device, which shows a comparable but overall the lowest leakage current. If the forward current is considered as well, the double and triple layers exhibit the best rectification of above 3 orders of magnitude in reverse and forward current bias, with acceptable forward currents.

The light J - V characteristics are shown in **Figure 6b**. As already expected from the work function, the device bearing only the WO_3 layer featured the lowest PV parameters, followed by bilayers. The triple layer exhibited only a slight lead over the state-of-the-art PEDOT:PSS layer. All PV parameters are shown in **Table 2**.

The statistical evaluation of all the solar cell parameters (obtained under illumination) is shown in **Figure 7**, and the

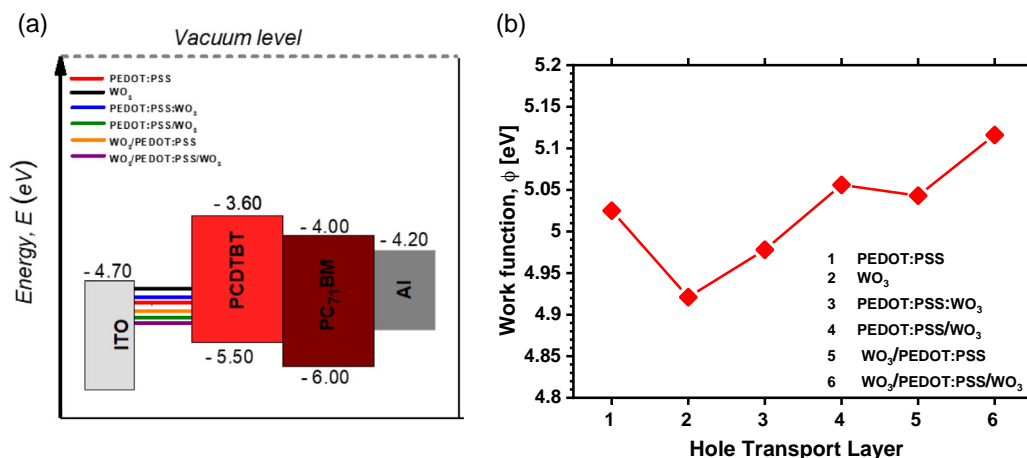


Figure 3. a) Energy-level diagram used in this work. b) Work function of the different HTL stacks.

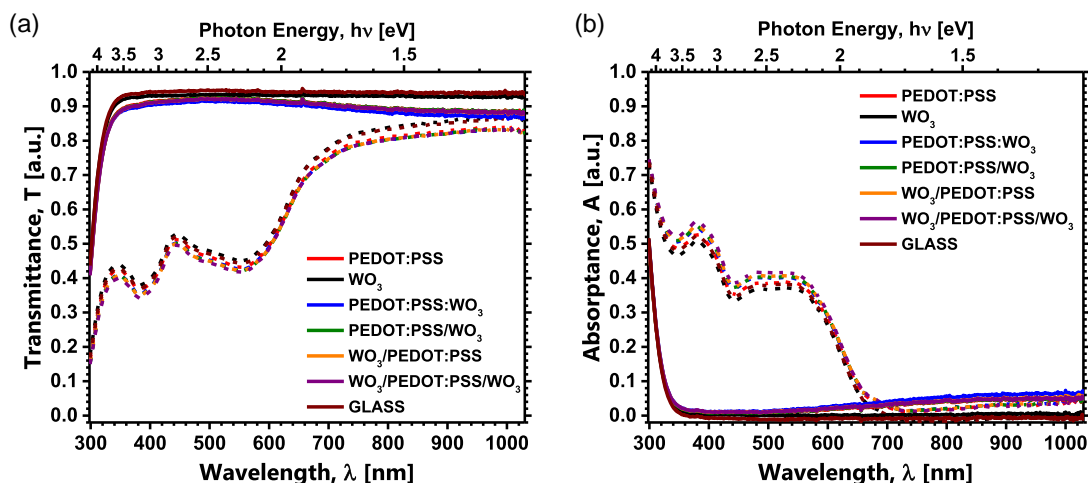


Figure 4. a) Transmittance spectra and b) absorbance spectra of films with various HTLs (solid line: pristine HTLs; dashed line: PAL PCDTBT:PC₇₁BM on top).

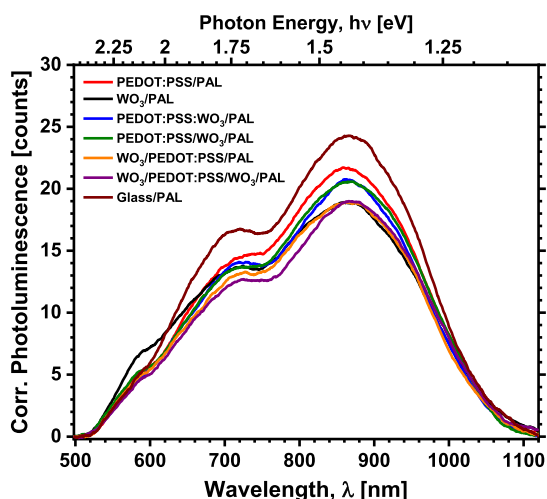


Figure 5. PL spectra of the films with PAL corrected at the excitation wavelength of the laser at 405 nm.

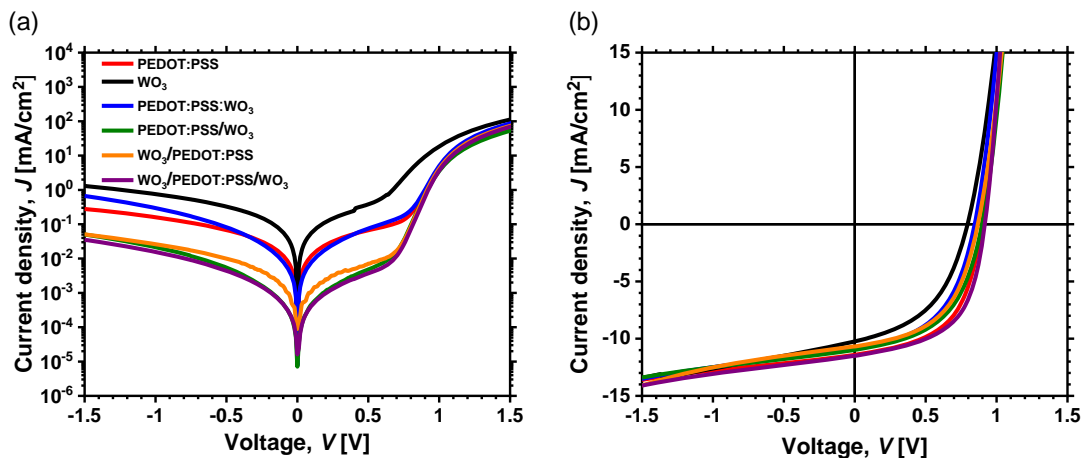


Figure 6. J–V characteristics of PCDTBT:PC₇₁BM solar cells with a systematic variation of the HTL: a) in the dark and b) under 1 sun illumination.

device performance parameters are shown in Table 2. The maximum values of the short-circuit current density values (J_{sc}) are more or less constant with a value around 11 mA cm^{-2} , only for the pristine WO_3 device, which shows a J_{sc} value of 1 mA cm^{-2} lower than the others. The maximum values of the open-circuit voltage (V_{oc}) are almost constant except for the pristine WO_3 device with a V_{oc} of 793 mV. We can also note here a small increase in the V_{oc} of the triple-layer device compared with the PEDOT:PSS one. The main change is on the maximum values of the parallel resistance (R_p), where the devices with the stacking layers of both pristine HTL materials have the highest R_p values. This result confirms the best selectivity and lowest leakage that we get from the dark J–V characteristics. For those double-layer and triple-layer devices, an increase in the series resistance (R_s) is observed, which causes a slight reduction in the fill factor (FF). The PCE calculated from the maximum values of the PCE after correction of the J_{sc} with the value obtained from the EQE measurement gives a value of 5.05% for the pristine PEDOT:PSS device. This value is 50% higher than the PCE value

Table 2. Photovoltaic parameters of the PCDTBT:PC₇₁BM solar cells exhibiting different HTLs in conventional architecture.

HTL	J_{sc} [mA cm^{-2}]	J_{sc_EQE} [mA cm^{-2}]	V_{oc} [mV]	FF [%]	PCE_{max} [%]	PCE_EQE [%]	R_s [Ω]	R_p [Ω]
PEDOT:PSS	11.06 ± 0.08	10.04	916 ± 23	55 ± 1.4	5.56 ± 0.17	5.05	9 ± 0.6	1230 ± 46
WO ₃	10.24 ± 0.06	9.00	793 ± 21	47 ± 0.8	3.79 ± 0.15	3.33	9 ± 0.5	800 ± 34
PEDOT:PSS:WO ₃	11.12 ± 0.09	10.01	895 ± 24	54 ± 1.5	5.46 ± 0.25	4.91	9 ± 0.6	1179 ± 51
PEDOT:PSS/WO ₃	11.04 ± 0.10	10.06	901 ± 18	53 ± 0.9	5.31 ± 0.27	4.84	10 ± 0.7	1320 ± 35
WO ₃ /PEDOT:PSS	10.98 ± 0.08	10.04	899 ± 23	53 ± 1.3	5.31 ± 0.28	4.86	10 ± 0.6	1389 ± 87
WO ₃ /PEDOT:PSS/WO ₃	11.13 ± 0.10	10.11	933 ± 26	53 ± 1.1	5.89 ± 0.30	5.35	11 ± 0.6	1472 ± 82

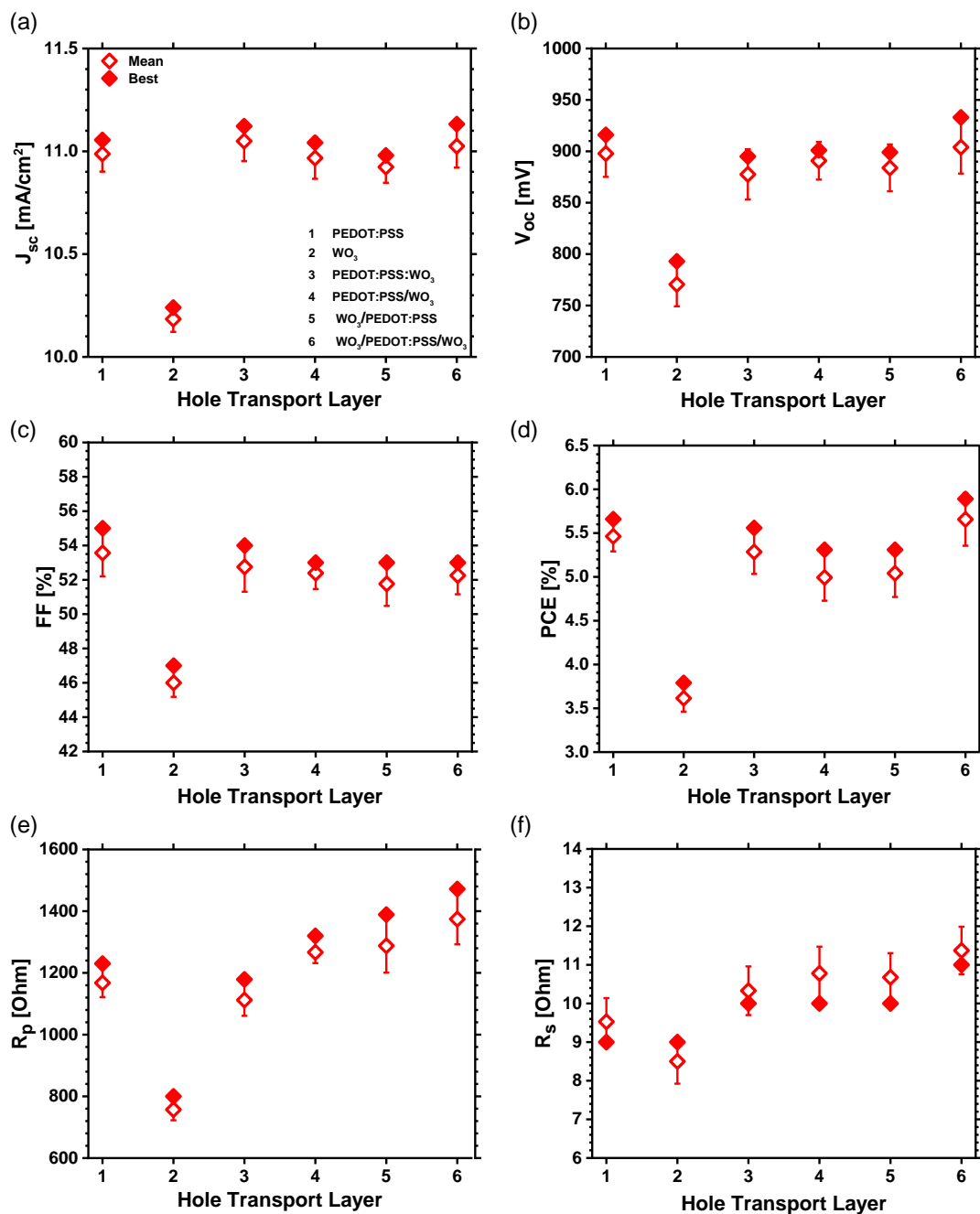


Figure 7. Statistical analysis of a) short-circuit current density, b) open-circuit voltage, c) FF, d) PCE, e) parallel resistance, and f) series resistance of PCDTBT:PC₇₁BM solar cells (20 devices) with a systematic variation of the HTL.

of the pristine WO_3 device, which exhibits a PCE of 3.33%. The blending device as well as the double-layer devices have similar efficiency as the PEDOT:PSS device. Indeed, when looking at the data (and variation of the same) of the photovoltaic parameters obtained for the triple layer in comparison with those obtained for PEDOT:PSS, there is no difference in the photocurrent generation, but the open-circuit voltage as well as the parallel resistance are significantly increased. In contrast, there is an improvement in the efficiency of the triple-layer device with a PCE value of 5.35%, which is 6% higher than the reference PEDOT:PSS device.

The spectral response of the devices is determined by the EQE measurements and is shown in **Figure 8a** and the calculated short-circuit current densities derived from those measurements are shown in Table 2. There are for all the devices except the pristine WO_3 device's similar spectral response (around 70%), with two peaks signals at 370 and 480 nm, which can be attributed to the interference effects. For the pristine WO_3 device, there is a shift in the position of the peak at 370 nm, and the peak at 480 nm completely disappears. This is probably caused by an interference effect due to the film thickness of WO_3 and the likely change in active layer thickness due to the WO_3 layer. **Figure 8b** shows the results of the electroluminescence spectra that were conducted to get a deeper insight into the bulk-heterojunction interface (charge transfer or CT state). The measurement consists of injecting charge carriers into the solar cell device by applying a 50 mA current in the forward direction and recording the fraction of electron-hole recombination that occurs radiatively. There was no noticeable electroluminescence signal detected for the pristine WO_3 injection layer, which might be due to the increased barrier between WO_3 and PAL, as WO_3 has a lower work function than all the other HTLs. All the other devices show a peak at 945 nm, which corresponds to the known CT-state energy of 1.31 eV.^[30] Moreover, the highest electroluminescence intensity was observed for the triple-layer device $\text{WO}_3/\text{PEDOT:PSS}/\text{WO}_3$. This may be due to improved hole injection in agreement with the larger work function. This result is also in line with the device performance, while this may not in general be the case, meaning that the higher electroluminescence intensity does not always refer to the higher-

performing device. In our case, the electroluminescence intensity can, however, be nicely correlated with the parallel resistance (R_p) values determined under illuminated I - V characterization.

To gain deeper insight into the type of charge recombination in the solar cells, we studied the light intensity dependence current-voltage characteristics (LID-IV). **Figure 9** shows the plot of the J_{sc} over the light intensity variation of the monochromatic LED light at the wavelength 520 nm in a log-log scale. Here, the intensity of the light was varied using different optical density filters and enabled us to span a range of four orders of magnitude. J_{sc} and light intensity are generally correlated by the following equation.

$$J_{sc} \propto I^\alpha \quad (1)$$

where I is the light intensity and α is the slope of linear fitting in the log-log plot.

The values of the slope α obtained from the different linear fits are close to unity, which indicates that bimolecular recombination does not limit the photocurrent.^[31-34]

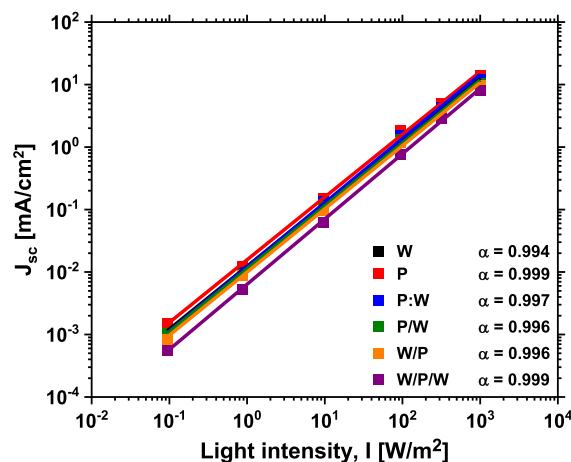


Figure 9. Log-log plots with the linear fits of the dependence of J_{sc} on the light intensity for PCDTBT:PC₇₁BM solar cells with various HTLs (monochromatic LED light with the wavelength 520 nm).

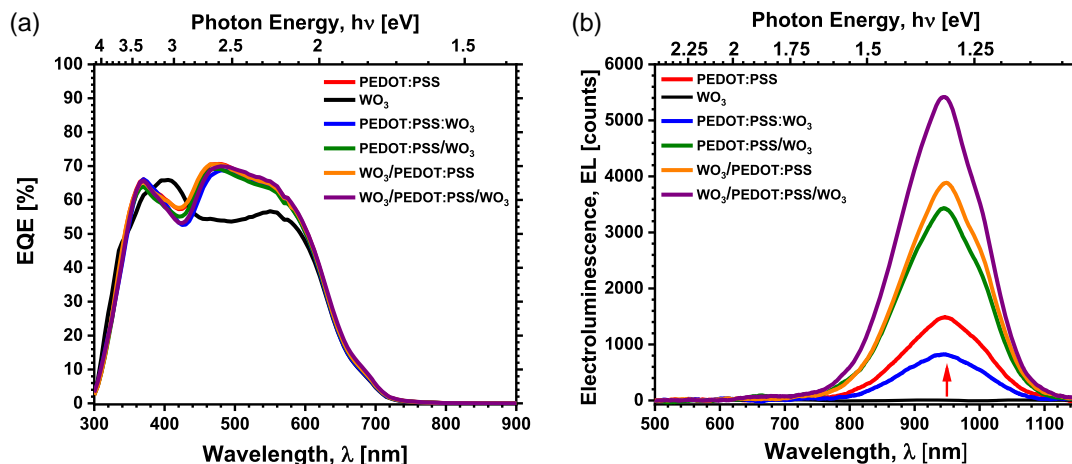


Figure 8. a) External quantum efficiency spectra and b) electroluminescence spectra of PCDTBT:PC₇₁BM solar cells.

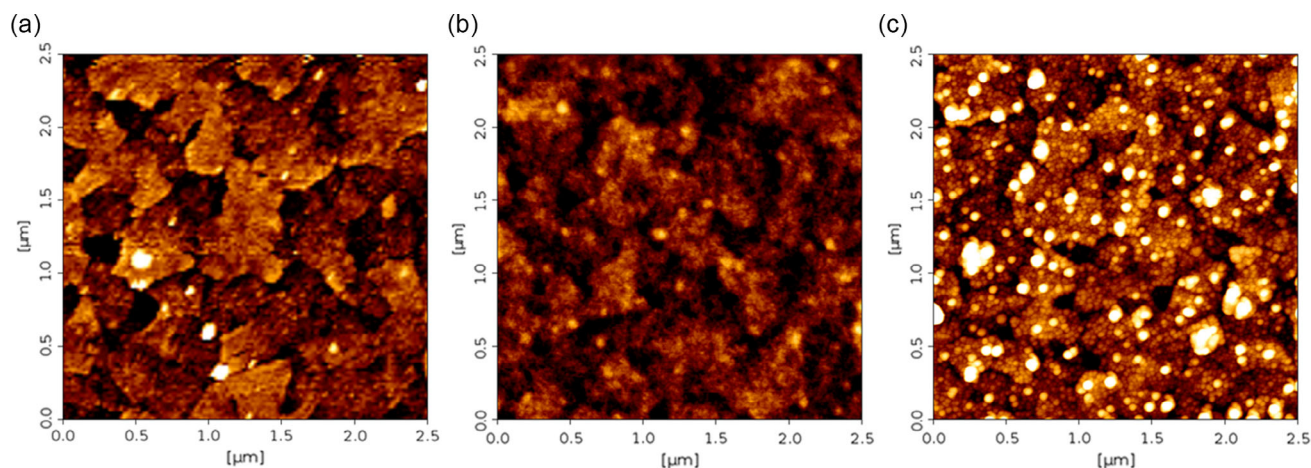


Figure 10. AFM images on ITO glass. a) bare ITO, b) PEDOT:PSS, and c) WO_3 .

To learn more about the layer structure and homogeneity of the various HTLs, AFM measurements were carried out. **Figure 10** shows the results for ITO, WO_3 , and PEDOT:PSS on the same substrate. It is evident that PEDOT:PSS even on top of ITO had a smoother surface than ITO. However, the same effect is not visible for the WO_3 film. Rather, inhomogeneous spots can be observed in case of WO_3 . When we compare the AFM image of WO_3 film on ITO glass and the one on bare glass (see Figure S4, Supporting Information), we can conclude that WO_3 precursor solution does not form a covering film on the ITO substrate. The origin of this is not clear at the moment, but it may be due to larger aggregates, which may form within the solution from which the WO_3 is cast. Furthermore, thickness measurements were carried out with laser-scanning microscopy. The average film thickness Δh (see **Table 3**) results from the mean value of the difference of the height profiles from area 1 and area 2, as shown in Figure S5, Supporting Information. There was not possible to determine the thickness of pristine WO_3 coated on bare glass. For the PEDOT:PSS and triple-layer WO_3 /PEDOT:PSS/ WO_3 films, the thickness values are the same. This indicates that no closed film is formed when casting WO_3 , confirming the observations of the AFM measurements. The same observation can be concluded for images obtained from the electroluminescence imaging (see Figure S6, Supporting Information), where inhomogeneous spots are also observed after casting of WO_3 precursor solution.

Solar cells were additionally aged under ISOS-L1 conditions. From these experiments, the burn-in times and lifetimes of these solar cells were evaluated and the completed aging data are included in Supporting Information. In regard to the lifetime, the triple-layer device shows an increased reproducibility, but there was no significant improvement observed for the use

of WO_3 , because the lifetime of the devices was limited by the electron-extracting contact.

4. Conclusion

In summary, we used a sol-gel approach to solution process WO_3 as a hole extraction layer in conventional PCDTBT:PC₇₁BM solar cells. AFM and laser scanning microscopy measurements indicate that there is not a closed film of WO_3 . This could be due to aggregation in solution or a wetting problem of the WO_3 precursor solution on top of the substrate, and hence we will pursue our work in the way solve this issue and obtain a uniform film. However, The *J*-*V* characteristics reveal a better contact selectivity and an improvement of the reverse current blocking behavior for the devices with the triple-layer WO_3 /PEDOT:PSS/ WO_3 configuration as the hole extraction layer compared with the reference devices with the pristine WO_3 and pristine PEDOT:PSS, resulting in the best device performance and significantly increased open-circuit voltage as well as parallel resistance. In terms of lifetime, the difference is also not so pronounced. However, the triple layer shows an increased reproducibility. This lifetime reproducibility combined with the improvement in the efficiency can be the keys for expectable revenue.

Supporting Information

Supporting Information is available from the Wiley Online Library or from the author.

Acknowledgements

H.H. and A.S.D. are grateful for financial support from the Deutsche Forschungsgemeinschaft (DFG) via the DFG project number 431903417. U.S.S. is grateful to the Thüringer Ministerium für Wirtschaft, Wissenschaft und Digitale Gesellschaft (TMWWDG) for funding the CEEC Jena. A.H. and T.P. thank the European Social Fund for Germany (ESF) for funding the project EilaSax (n° 100339506). The authors appreciate for atomic force microscopy measurements supported by Susanne Sandkuhl at the FSU Jena.

Open access funding enabled and organized by Projekt DEAL.

Table 3. Thickness values of different HTL films coated on bare glass.

HTL film	Thickness Δh [nm]
PEDOT:PSS	45.7
WO_3 /PEDOT:PSS/ WO_3	46.0

Conflict of Interest

The authors declare no conflict of interest.

Data Availability Statement

The data that support the findings of this study are available from the corresponding authors upon reasonable request.

Keywords

hole transport layers, metal oxides, polymer solar cells

Received: June 2, 2021

Revised: September 30, 2021

Published online: October 17, 2021

-
- [1] National Renewable Energy Laboratory (NREL), *Best research-cell efficiency chart*, <https://www.nrel.gov/pv/cell-efficiency.html> (accessed: May, 2021).
- [2] C. J. Brabec, M. Heeney, I. McCulloch, J. Nelson, *Chem. Soc. Rev.* **2011**, *40*, 1185.
- [3] M. A. Ruderer, P. Müller-Buschbaum, *Soft Matter* **2011**, *7*, 5482.
- [4] H. Hoppe, N. S. Sariciftci, *J. Mater. Chem.* **2006**, *16*, 45.
- [5] M. P. De Jong, L. J. Van Ijzendoorn, M. J. A. De Voigt, *Appl. Phys. Lett.* **2000**, *77*, 2255.
- [6] K. Sun, S. Zhang, P. Li, Y. Xia, X. Zhang, D. Du, F. H. Isikgor, J. Ouyang, *J. Mater. Sci.: Mater. Electron.* **2015**, *26*, 4438.
- [7] L. Bießmann, L. P. Kreuzer, T. Widmann, N. Hohn, J.-F. Moulin, P. Müller-Buschbaum, *ACS Appl. Mater. Interfaces* **2018**, *10*, 9865.
- [8] Y. Wang, W. Lan, N. Li, Z. Lan, Z. Li, J. Jia, F. Zhu, *Adv. Energy Mater.* **2019**, *9*, 1900157.
- [9] M. Jørgensen, K. Norrman, F. C. Krebs, *Sol. Energy Mater. Sol. Cells* **2008**, *92*, 686.
- [10] A. Anand, J. P. Madalaimuthu, M. Schaal, F. Otto, M. Gruenewald, S. Alam, T. Fritz, U. S. Schubert, H. Hoppe, *ACS Appl. Electron. Mater.* **2021**, *3*, 929.
- [11] K. X. Steirer, P. F. Ndione, N. E. Widjonarko, M. T. Lloyd, J. Meyer, E. L. Ratcliff, A. Kahn, N. R. Armstrong, C. J. Curtis, D. S. Ginley, J. J. Berry, D. C. Olson, *Adv. Energy Mater.* **2011**, *1*, 813.
- [12] K. Zilberberg, H. Gharbi, A. Behrendt, S. Trost, T. Riedl, *ACS Appl. Mater. Interfaces* **2012**, *4*, 1164.
- [13] T. Stubhan, N. Li, N. A. Luechinger, S. C. Halim, G. J. Matt, C. J. Brabec, *Adv. Energy Mater.* **2012**, *2*, 1433.
- [14] H. Choi, B. Kim, M. J. Ko, D.-K. Lee, H. Kim, S. H. Kim, K. Kim, *Org. Electron.* **2012**, *13*, 959.
- [15] T. Yamanari, T. Taima, J. Sakai, J. Tsukamoto, Y. Yoshida, *Jpn. J. Appl. Phys.* **2010**, *49*, 01AC02.
- [16] S. Chen, J. R. Manders, S.-W. Tsang, F. So, *J. Mater. Chem.* **2012**, *22*, 24202.
- [17] S. Höfle, M. Bruns, S. Strässle, C. Feldmann, U. Lemmer, A. Colmann, *Adv. Mater.* **2013**, *25*, 4113.
- [18] S. B. Lee, J. Ho Beak, B. H. Kang, K.-Y. Dong, Y.-Y. Yu, Y. Doo Lee, B.-K. Ju, *Sol. Energy Mater. Sol. Cells* **2013**, *117*, 203.
- [19] S. Han, W. S. Shin, M. Seo, D. Gupta, S.-J. Moon, S. Yoo, *Org. Electron.* **2009**, *10*, 791.
- [20] M. G. Varnamkhasti, E. Shahriaria, *J. Eur. Opt. Soc. Rapid Publ.* **2015**, *10*.
- [21] L. Chen, C. Xie, Y. Chen, *Adv. Funct. Mater.* **2014**, *24*, 3986.
- [22] F. Guillain, D. Tsikritzis, G. Skoulatakis, S. Kennou, G. Wantz, L. Vignau, *Sol. Energy Mater. Sol. Cells* **2014**, *122*, 251.
- [23] S. J. Lee, A. R. Bin Mohd Yusoff, J. Jang, *RSC Adv.* **2014**, *4*, 20242.
- [24] Z. A. Tan, L. Li, C. Cui, Y. Ding, Q. Xu, S. Li, D. Qian, Y. Li, *J. Phys. Chem. C* **2012**, *116*, 18626.
- [25] M. Qiu, D. Zhu, X. Bao, J. Wang, X. Wang, R. Yang, *J. Mater. Chem. A* **2016**, *4*, 894.
- [26] W. Kim, J. Kyu Kim, Y. Lim, I. Park, Y. Suk Choi, J. Hyeok Park, *Sol. Energy Mater. Sol. Cells* **2014**, *122*, 24.
- [27] M. O. Reese, S. A. Gevorgyan, M. Jørgensen, E. Bundgaard, S. R. Kurtz, D. S. Ginley, D. C. Olson, M. T. Lloyd, P. Morvillo, E. A. Katz, A. Elschner, O. Haillant, T. R. Currier, V. Shrotriya, M. Hermenau, M. Riede, K. R. Kirov, G. Trimmel, T. Rath, O. Inganäs, F. Zhang, M. Andersson, K. Tvingstedt, M. Lira-Cantu, D. Laird, C. McGuinness, S. Gowrisanker, M. Pannone, M. Xiao, J. Hauch, et al., *Sol. Energy Mater. Sol. Cells* **2011**, *95*, 1253.
- [28] M. V. Khenkin, E. A. Katz, A. Abate, G. Bardizza, J. J. Berry, C. Brabec, F. Brunetti, V. Bulović, Q. Burlingame, A. Di Carlo, R. Cheacharoen, Y.-B. Cheng, A. Colmann, S. Cros, K. Domanski, M. Dusza, C. J. Fell, S. R. Forrest, Y. Galagan, D. Di Girolamo, M. Grätzel, A. Hagfeldt, E. von Hauff, H. Hoppe, J. Kettle, H. Köbler, M. S. Leite, S. Liu, Y.-L. Loo, J. M. Luther, et al., *Nat. Energy* **2020**, *5*, 35.
- [29] R. Roesch, T. Faber, E. von Hauff, T. M. Brown, M. Lira-Cantu, H. Hoppe, *Adv. Energy Mater.* **2015**, *5*, 24.
- [30] O. Synooka, K.-R. Eberhardt, C. R. Singh, F. Hermann, G. Ecker, B. Ecker, E. Von Hauff, G. Gobsch, H. Hoppe, *Adv. Energy Mater.* **2014**, *4*, 1300981.
- [31] I. Riedel, J. Parisi, V. Dyakonov, L. Lutsen, D. Vanderzande, J. C. Hummelen, *Adv. Funct. Mater.* **2004**, *14*, 38.
- [32] P. Schilinsky, C. Waldauf, C. J. Brabec, *Appl. Phys. Lett.* **2002**, *81*, 3885.
- [33] J. K. J. Van Duren, X. Yang, J. Loos, C. W. T. Bulle-Lieuwma, A. B. Sieval, J. C. Hummelen, R. A. J. Janssen, *Adv. Funct. Mater.* **2004**, *14*, 425.
- [34] L. J. A. Koster, V. D. Mihailetschi, H. Xie, P. W. M. Blom, *Appl. Phys. Lett.* **2005**, *87*, 203502.